Article

Cell

The BRAF Pseudogene Functions as a Competitive Endogenous RNA and Induces Lymphoma In Vivo

Graphical Abstract

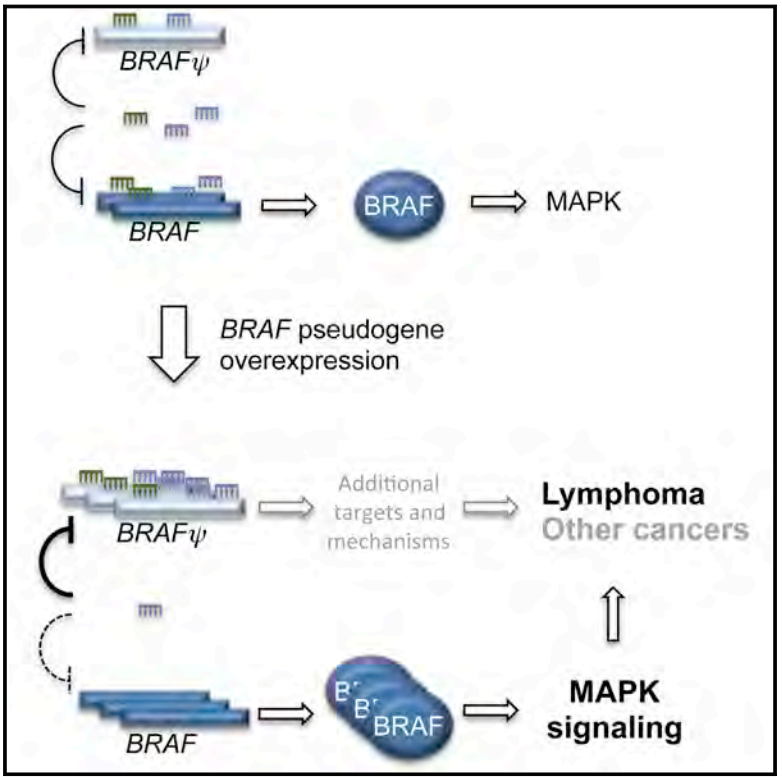

Authors

Florian A. Karreth, Markus Reschke, ..., Roberto Chiarle, Pier Paolo Pandolfi

Correspondence

ppandolf@bidmc.harvard.edu

In Brief

The in vivo evidence for the regulatory activity of pseudogenes has been lacking, and their role in disease progression has been correlative. This study now shows that transgenic expression of the BRAF pseudogene induces a malignancy in mice resembling human diffuse large B cell lymphoma, establishing its oncogenic function.

Highlights

- The BRAF pseudogene functions as a ceRNA for BRAF in humans and mice
- *Braf-rs1* overexpression promotes B cell lymphoma in mice
- Silencing of *BRAFP1* affects MAPK signaling and proliferation of human cancer cells
- Genomic gains and aberrant expression of *BRAFP1* are found in various human cancers

Karreth et al., 2015, Cell *161*, 319–332
April 9, 2015
http://dx.doi.org/10.1016/j.cell.2015.02.043

CellPress

Cell

The BRAF Pseudogene Functions as a Competitive Endogenous RNA and Induces Lymphoma In Vivo

Florian A. Karreth,[1] Markus Reschke,[1] Anna Ruocco,[1] Christopher Ng,[1] Bjoern Chapuy,[2] Valentine Léopold,[1] Marcela Sjoberg,[3] Thomas M. Keane,[3] Akanksha Verma,[4] Ugo Ala,[1] Yvonne Tay,[1,9] David Wu,[5] Nina Seitzer,[1] Martin Del Castillo Velasco-Herrera,[3] Anne Bothmer,[1] Jacqueline Fung,[1] Fernanda Langellotto,[6] Scott J. Rodig,[7] Olivier Elemento,[4] Margaret A. Shipp,[2] David J. Adams,[3] Roberto Chiarle,[6,8] and Pier Paolo Pandolfi[1,*]

[1]Cancer Research Institute, Beth Israel Deaconess Cancer Center, Department of Medicine and Pathology, Beth Israel Deaconess Medical Center, Harvard Medical School, Boston, MA 02215, USA

[2]Department of Medical Oncology, Dana-Farber Cancer Institute, Boston, MA 02115, USA

[3]Experimental Cancer Genetics, Wellcome Trust Sanger Institute, Wellcome Trust Genome Campus, Hinxton CB10 1HH, UK

[4]Department of Physiology and Biophysics, Institute for Computational Biomedicine, Weill Cornell Medical College, New York, NY 10021, USA

[5]Meyer Cancer Center, Weill Cornell Medical College, New York, NY 10021, USA

[6]Department of Pathology, Children's Hospital and Harvard Medical School, Boston, MA 02115, USA

[7]Department of Pathology, Brigham and Women's Hospital, Boston, MA 02115, USA

[8]Department of Molecular Biotechnology and Health Sciences, University of Torino, 10124 Torino, Italy

[9]Present address: Cancer Science Institute of Singapore and Department of Biochemistry, Yong Loo Lin School of Medicine, National University of Singapore, Singapore 117597

*Correspondence: ppandolf@bidmc.harvard.edu

http://dx.doi.org/10.1016/j.cell.2015.02.043

SUMMARY

Research over the past decade has suggested important roles for pseudogenes in physiology and disease. In vitro experiments demonstrated that pseudogenes contribute to cell transformation through several mechanisms. However, in vivo evidence for a causal role of pseudogenes in cancer development is lacking. Here, we report that mice engineered to overexpress either the full-length murine *B-Raf* pseudogene *Braf-rs1* or its pseudo "CDS" or "3′ UTR" develop an aggressive malignancy resembling human diffuse large B cell lymphoma. We show that *Braf-rs1* and its human ortholog, *BRAFP1*, elicit their oncogenic activity, at least in part, as competitive endogenous RNAs (ceRNAs) that elevate BRAF expression and MAPK activation in vitro and in vivo. Notably, we find that transcriptional or genomic aberrations of *BRAFP1* occur frequently in multiple human cancers, including B cell lymphomas. Our engineered mouse models demonstrate the oncogenic potential of pseudogenes and indicate that ceRNA-mediated microRNA sequestration may contribute to the development of cancer.

INTRODUCTION

Over the past few years, remarkable progress has been made in establishing long non-coding RNAs (lncRNAs) as important regulators of various biological processes. Given their critical roles, it is not surprising that aberrant expression and/or function of lncRNAs are implicated in the development of diseases such as cancer (Gutschner and Diederichs, 2012).

Pseudogenes, a sub-class of lncRNA genes that developed from protein-coding genes but have lost the ability to produce proteins, have long been viewed as non-functional genomic relicts of evolution (Poliseno, 2012). However, the vast majority of pseudogenes have protein-coding parental counterparts with which they share high sequence homology, which enables pseudogenes to participate in posttranscriptional regulation of their parental genes. Mechanisms of parental gene regulation include the formation of endogenous siRNAs (Tam et al., 2008; Watanabe et al., 2008), recruitment of regulatory proteins by pseudogene antisense RNAs to complementary sites in the parental gene to modulate chromatin remodeling and transcription (Hawkins and Morris, 2010; Johnsson et al., 2013), and competition for RNA-binding proteins or the translation machinery (Bier et al., 2009; Chiefari et al., 2010; Han et al., 2011).

We recently proposed that the high sequence homology enables pseudogenes to compete with their parental genes for a shared pool of common microRNAs (miRNAs) (Poliseno et al., 2010), thus regulating the latter's expression as competitive endogenous RNA (ceRNAs) (Salmena et al., 2011). This mechanism is of particular relevance to cancer where pseudogenes are aberrantly expressed (Kalyana-Sundaram et al., 2012). Specifically, we demonstrated that pseudogenes of the frequently mutated cancer genes *PTEN* and *KRAS* function as ceRNAs in vitro (Poliseno et al., 2010). Moreover, we and others reported that mRNAs and non-coding RNAs may serve as ceRNAs that regulate each other through miRNA-dependent crosstalk (Cazalla et al., 2010; Cesana et al., 2011; Franco-Zorrilla et al.,

2007; Hansen et al., 2013; Karreth et al., 2011; Libri et al., 2012; Marcinowski et al., 2012; Memczak et al., 2013; Sumazin et al., 2011; Tay et al., 2011; Wang et al., 2013), suggesting that pseudogenes regulate the expression of their parental genes in the context of larger networks of protein-coding and non-coding ceRNAs.

While sufficient data exist to demonstrate pseudogene functions in vitro, in vivo evidence for the regulatory activity of pseudogenes—either as ceRNAs or by any of the other above-mentioned mechanisms—is lacking, and their role in disease progression is correlative. Here, we describe a causal role for the *BRAF* pseudogene in the development of cancer.

RESULTS

The BRAF Pseudogene Regulates BRAF in a Dicer1-Dependent Manner

The BRAF pseudogene (*BRAFP1*) is overexpressed in various tumor types (Zou et al., 2009; Kalyana-Sundaram et al., 2012), suggesting that it may contribute to cancer development. We have shown that pseudogenes are able to regulate expression of their parental genes through sequestration of shared miRNAs (Poliseno et al., 2010), and *BRAFP1*-mediated elevation of BRAF may promote MAPK signaling and tumorigenesis. MiRNA predictions revealed that murine *Braf-rs1* (Gm18189) and *B-Raf* are targeted by 54 and 114 miRNA families, respectively, 53 of which they have in common. Similarly, human *BRAFP1* and *BRAF* are targeted by 60 and 48 miRNA families, respectively, and share 40 (Figures S1A–S1D, Table S1). Thus, the *BRAF* pseudogene may operate as a ceRNA for BRAF in mice and humans. Indeed, ectopic expression of *Braf-rs1* in NIH 3T3 fibroblasts and *BRAFP1* in human PC9 and HeLa cancer cells elevated BRAF protein and ERK phosphorylation (Figures 1A and S1E). Importantly, B-Raf was critical for this effect, as the *Braf-rs1*-induced increase in pERK was negated by genetic deletion of *B-Raf* in *B-Raf*$^{fl/fl}$ fibroblasts (Figure 1B). Moreover, expression of the *BRAF* pseudogene increased proliferation of NIH 3T3, PC9, and HeLa cells (Figures 1C, 1D, and S1F). Moderate B-Raf overexpression was sufficient to increase pERK expression, proliferation, and anchorage-independent growth of NIH 3T3 fibroblasts (Figures S1G–S1I), indicating that *Braf-rs1*-mediated elevation of B-Raf may be sufficient for the observed phenotype.

To test whether the effect of the *BRAF* pseudogene on BRAF expression and proliferation rates was dependent on miRNAs, we utilized cell lines lacking functional Dicer1, a ribonuclease critical for miRNA biogenesis and whose deficiency results in drastically reduced levels of mature miRNAs (Cummins et al., 2006; Ravi et al., 2012). Ectopic expression of *Braf-rs1* increased expression of B-Raf and pERK and elevated proliferation of Dicer1-proficient murine sarcoma cells, but not that of isogenic Dicer1 knockout cells (Figures 1E and 1F). Similarly, overexpression of *BRAFP1* in Dicer1-proficient human HCT116 colon cancer cells increased expression of BRAF and pERK and elevated proliferation, and these effects were abrogated in isogenic Dicer1 mutant HCT116 cells (Figures 1G and 1H). Thus, the *BRAF* pseudogene-induced effects are dependent on BRAF and Dicer1.

The *BRAF* Pseudogene Regulates BRAF as a Competitive Endogenous RNA

The finding that the *BRAF* pseudogene mediates its effect through mature miRNAs suggests that it may function as a ceRNA. To test this directly, we co-expressed *BRAFP1* with a human *BRAF*-3′ UTR-luciferase reporter in Dicer1-proficient and -deficient HCT116 cells. *BRAFP1* elevated the activity of the *BRAF* 3′ UTR-luciferase reporter in a Dicer1-dependent manner (Figure 2A), further supporting the notion that the crosstalk is mediated by mature miRNAs. To validate this result, we tested several predicted shared miRNAs in 3′ UTR-luciferase reporter assays. Three out of ten murine miRNAs (miR-134, miR-543, and miR-653) significantly repressed *Braf-rs1* and *B-Raf* luciferase reporters (Figure 2B), suggesting that the crosstalk may be mediated at least in part by these three miRNAs.

Next, we determined the ability of *Braf-rs1* to decoy the dual targeting miRNAs miR-134, miR-543, and miR-653 from luciferase reporters carrying miRNA response elements (MREs). *Braf-rs1* regulated the expression of the luciferase reporters, especially at lower miRNA concentrations (Figure 2C). *Braf-rs1*-mediated sequestration of the least potent of the three dual targeting miRNAs, miR-543, had the most robust effect on luciferase reporter activity (Figure 2C). These data suggest that both potency and abundance of the miRNAs may be important determinants for ceRNA crosstalk. In addition, *Braf-rs1* was able to sequester endogenous miR-653, miR-134, and miR-543 from the respective luciferase-MRE reporters, and mutation of the MREs in *Braf-rs1* abrogated this effect (Figure 2D). Similarly, four out of nine human miRNAs (miR-30a, miR-182, miR-876, and miR-590) were able to repress *BRAF*- and *BRAFP1*-luciferase reporters (Figure S2A). miR-30a, miR-182, and miR-876 were also efficiently sequestered from the respective MRE-luciferase reporters by *BRAFP1*, and mutation of these miRNA-binding sites reduced *BRAFP1*'s activity as a miRNA sponge (Figure S2B).

Generation of TRE-BPS Mice

As *Braf-rs1* regulates the expression of *B-Raf* and MAPK signaling, we sought to investigate whether aberrant *Braf-rs1* expression is oncogenic in vivo. To this end, we generated a transgenic allele containing murine *Braf-rs1* under the control of a doxycycline (Dox)-inducible Tet-response element (TRE) and targeted it to the collagen A1 locus using Flp recombinase-mediated genomic integration (Beard et al., 2006) (Figures S2C and S2D). We isolated mouse embryonic fibroblasts (MEFs) from TRE-Braf-rs1 (henceforth referred to as TRE-BPS) mice to confirm that expression of the *Braf-rs1* allele regulates B-Raf. Infection of MEFs with a tTA-expressing retrovirus resulted in 6- to 18-fold induction *of Braf-rs1* expression (Figures 2E and S2E), as well as increased levels of B-Raf and pERK (Figure 2F) and proliferation (Figure 2G), confirming that the transgenic allele elicits effects similar to ectopic expression of *Braf-rs1*.

We used TRE-BPS MEFs to analyze the stoichiometry of *B-Raf* and *Braf-rs1.* First, we determined the absolute number of transcripts by qPCR using plasmids carrying *Braf-rs1* and *B-Raf* as standards (Figure S2E). In TRE-BPS MEFs infected with a control retrovirus, *B-Raf* molecules were 13- to 26-fold more abundant than *Braf-rs1*, while in tTA-infected cells, the *B-Raf*:*Braf-rs1* ratio

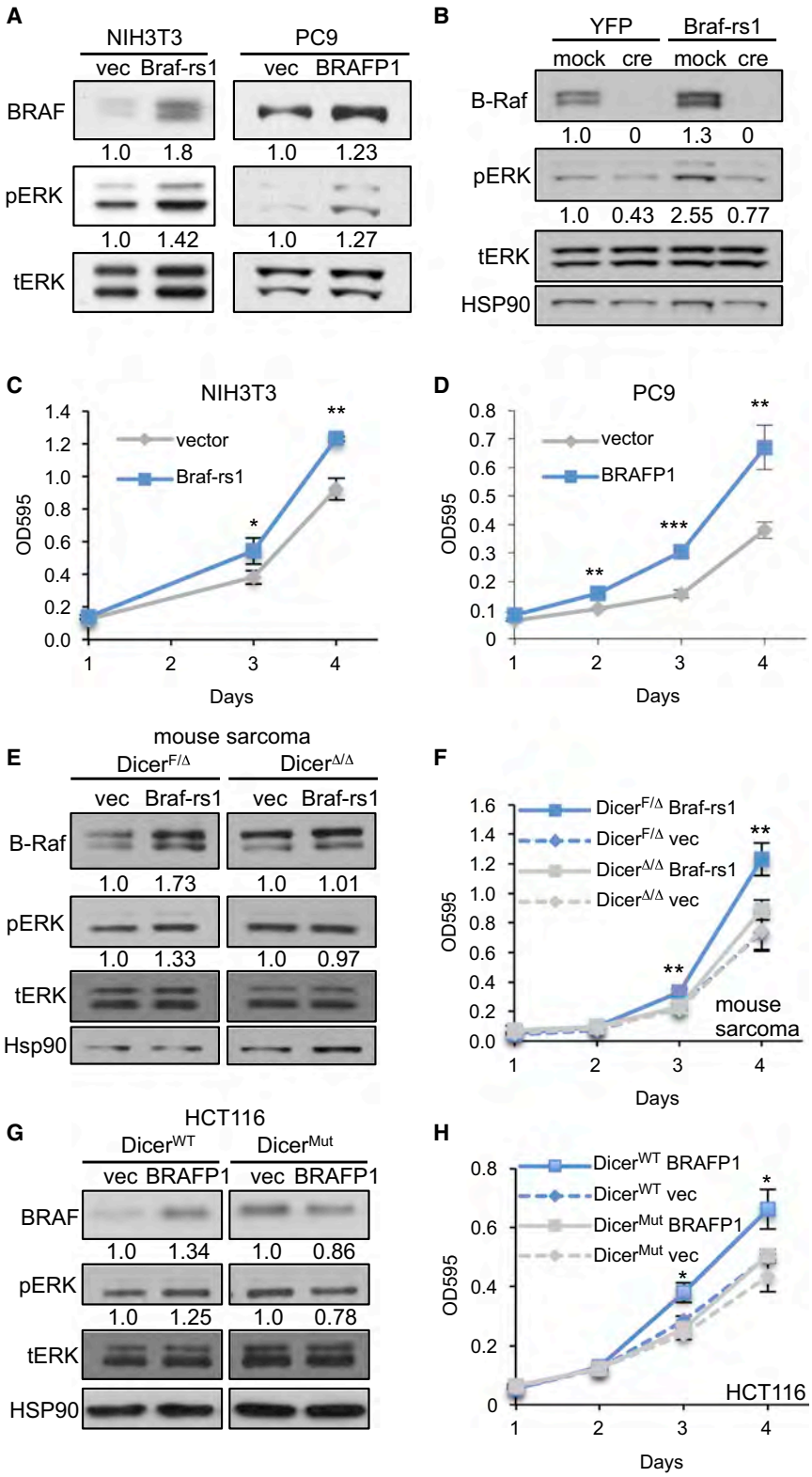

Figure 1. The *BRAF* Pseudogene Regulates BRAF in a Dicer1-Dependent Manner

(A) Western blot demonstrating increased BRAF and pERK expression upon ectopic *BRAF* pseudogene expression in mouse (NIH 3T3, left) and human (PC9, right) cells.

(B) Western blot of *B-Raf*$^{fl/fl}$ fibroblasts overexpressing *Braf-rs1* or control (yellow fluorescent protein [YFP]) in the presence or absence of Adeno-Cre infection.

(C) Increased proliferation of NIH 3T3 fibroblasts upon ectopic *Braf-rs1* expression.

(D) Increased proliferation of PC9 cells upon ectopic *BRAFP1* expression.

(E and F) Western blot (E) and proliferation assay (F) of *Dicer1*$^{FL/\Delta}$ and *Dicer1*$^{\Delta/\Delta}$ murine sarcoma cells overexpressing *Braf-rs1*.

(G and H) Western blot (G) and proliferation assay (H) of *Dicer1*^{WT} and *Dicer1*^{Mut} human HCT116 colon cancer cells overexpressing *BRAFP1*.

Error bars represent mean ± SD. *p ≤ 0.05; **p ≤ 0.01; ***p ≤ 0.001. See also Figure S1.

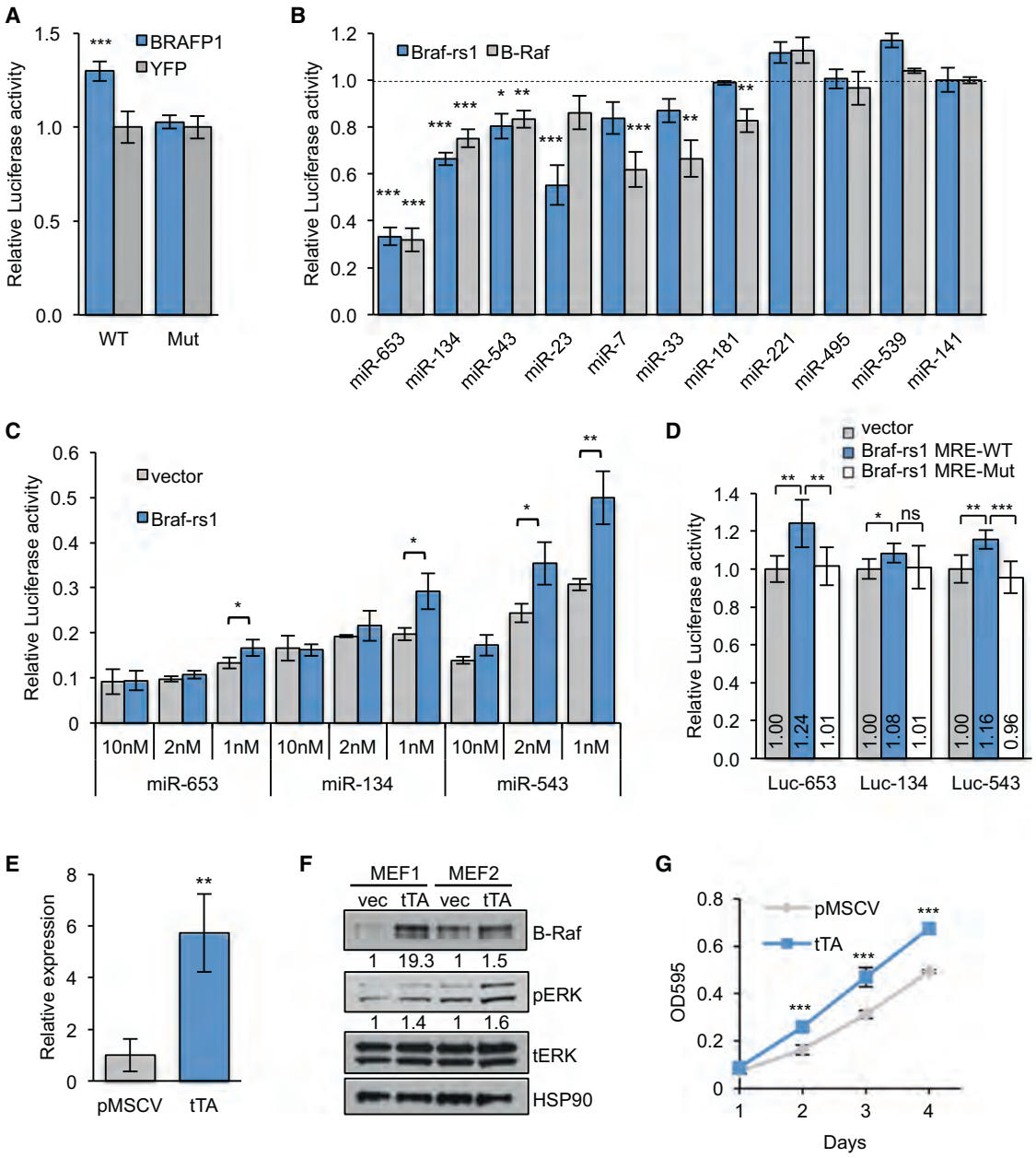

Figure 2. The *BRAF* Pseudogene Functions as a miRNA Sponge

(A) BRAF 3′ UTR-luciferase reporter assay in Dicer1^{WT} and Dicer1^{Mut} HCT116 cells expressing *BRAFP1* or control (YFP).

(B) Luciferase reporter assay using the 3′ UTRs of *B-Raf* and *Braf-rs1* to analyze repression by the indicated miRNA mimics. miR141 serves as a negative control.

(C) *Braf-rs1* sequesters miRNAs to regulate MRE-Luc reporter activity. HEK293T cells were co-transfected with MRE-Luc reporter constructs, the respective miRNA mimics, and Braf-rs1-L277 or empty control L277 plasmids. The luciferase activity relative to a Luc reporter without MRE is shown.

(D) Luciferase activity measured in HEK293T cells co-expressing MRE-Luc reporters (Luc-653, Luc-134, or Luc-543) and wild-type or MRE mutant *Braf-rs1* or empty vector.

(E) qPCR showing tTA-induced *Braf-rs1* expression in TRE-BPS MEFs.

(F) Western blot for B-Raf and pERK in tTA-infected TRE-BPS MEFs.

(G) Proliferation of TRE-BPS MEF1 shown in (F).

Error bars represent mean ± SD. *p ≤ 0.05; **p ≤ 0.01; ***p ≤ 0.001. See also Figure S2.

was between 1.3 and 2.5 (Figure S2E). RNA-sequencing (RNA-seq) analysis confirmed *Braf-rs1* induction and found *B-Raf:Braf-rs1* ratios in a range similar to that determined by qPCR (Figure S2F and data not shown). Next, we determined the number of molecules of miR-653, miR-134, and miR-543 in TRE-BPS MEFs by qPCR using standard curves. MiRNA expression was not

significantly affected upon transgene induction (Figure S2G, Table S2). Mir-653 was expressed at extremely low levels, likely precluding it from *Braf*-rs1/*B-Raf* ceRNA crosstalk in MEFs. Additional predicted miRNAs that are expressed in MEFs (Table S2) but were not further validated may also contribute to crosstalk. Hence, the stoichiometry of *B-Raf*, transgenic *Braf-rs1*, and some dual-targeting miRNAs fits well within the optimal crosstalk criteria that we have recently established (Ala et al., 2013), supporting the hypothesis that overexpression of *Braf-rs1* increases B-Raf through its ceRNA activity.

Braf-rs1 Causes Diffuse Large B Cell Lymphoma

To induce global overexpression of *Braf-rs1* in vivo, TRE-BPS mice were crossed to CAG-rtTA3 mice (Premsrirut et al., 2011), and compound mutant animals and single mutant controls were placed on a Dox-containing diet at 3 weeks of age (Figure S3A). qPCR analysis after 4 weeks of Dox administration confirmed *Braf-rs1* overexpression in all organs tested (Figure S3B). Following 4 months of Dox treatment, TRE-BPS; CAG-rtTA3 mice became moribund and had to be sacrificed after a median survival of 421 days (Figure 3A), while none of the single-mutant animals or compound mutants maintained on a regular diet developed similar symptoms. All moribund TRE-BPS; CAG-rtTA3 mice presented with splenomegaly (Figures 3B and 3C) and enlarged lymph nodes (Figure 3K).

Histological analysis revealed large tumor nodules involving the splenic white pulp (Figures 3D and 3E). Tumors consisted of large lymphoid cells admixed with numerous plasmablasts and plasma cells (Figure 3F). The mitotic rate was very high (Figure 3F), and the proliferation rate was markedly increased compared to normal white pulp (Figures 3G and S3C).

We determined the immunophenotype of the splenic tumors by flow cytometry when TRE-BPS; CAG-rtTA3 mice succumbed to the malignancy. The cell population expressing surface B220 was decreased in spleens (Figure 3H), while Gr-1$^+$/Mac-1$^+$ cells were slightly increased and CD3$^+$ cells were unchanged (Figures 3I and 3J). Lymph nodes displayed more B220$^+$ cells, while CD3$^+$ cells were less abundant (Figures 3L and 3M). Similar results were obtained when calculated as fold change relative to controls (Figures S3D–S3H). By immunohistochemistry, tumor cells stained positively for CD45R/B220 and IgG (Figures 4A and 4C) and negatively for CD3 (Figure 4B). Moreover, tumors were negative for the germinal center marker Bcl6 (Figure 4D) and strongly positive for Mum1 (Figure 4E), while residual germinal centers adjacent to the tumors were Bcl6 positive and Mum1 negative (Figures 4D and 4E). The decrease of B220 expression on the surface of tumor cells reflected the marked plasmacellular differentiation, as shown by the abundance of IgG$^+$ cells. Overall, this phenotype was consistent with post-germinal center diffuse large B cell lymphoma.

We next determined the abundance of *Braf-rs1*, *B-Raf*, and miRNA molecules in spleens after short-term Dox exposure (10 days) and in lymphomas and control spleens after long-term Dox exposure. While endogenous *Braf-rs1* expression was between 6- and 115-fold lower than *B-Raf*, expression of transgenic *Braf-rs1* was comparable to *B-Raf* (Figures S3I–S3L). Expression of miR-134, miR-543, and miR-653 was not affected by *Braf-rs1* overexpression (Figures S3M and S3N). Similar to MEFs, miR-653 was expressed at low levels, while miR-134 and miR-543 were expressed at levels that are amenable to ceRNA crosstalk (Figures S3M and S3N).

Aggressive Lymphomas Are Transplantable and Depend on *Braf-rs1* Expression

Macroscopic lymphoma nodules were commonly observed in the kidneys, livers, and lungs of TRE-BPS; CAG-rtTA3 mice (Figure 4F and data not shown), and histological analysis revealed microscopic organ infiltration by lymphoma cells in all animals (Figures 4G–4I). Such tumor cells displayed a CD45R/B220$^+$ and Mum1$^+$ phenotype identical to the cells infiltrating spleens and lymph nodes (Figures 4J–4O). Additionally, heterozygous loss of *Pten* reduced the median survival of TRE-BPS; CAG-rtTA3 mice to 172 days (data not shown).

To further assess the tumorigenicity of *Braf-rs1*-induced lymphomas, we analyzed their transplantation potential. NSG mice injected with TRE-BPS; CAG-rtTA3 spleen cells had to be sacrificed 100–150 days after transplantation due to deteriorating health. Moreover, NSG mice transplanted with TRE-BPS; CAG-rtTA3; *Pten*$^{+/-}$ lymphoma cells had to be sacrificed after 80 days (data not shown). NSG recipients exhibited infiltrating lymphoma cells in spleens, livers, lungs, and kidneys (Figure 5A). These results suggest that *Braf-rs1*-induced lymphomas are transplantable and highly aggressive.

We next determined whether continuous expression of *Braf-rs1* was required for tumor maintenance. TRE-BPS; CAG-rtTA3 receiving a Dox-diet were monitored by palpation and were taken off Dox chow once splenomegaly became apparent. Spleen sizes of these animals were subsequently measured using high-resolution ultrasound. Notably, enlarged spleens of all TRE-BPS; CAG-rtTA3 mice reduced in size, while spleens of control mice were unaffected (Figure 5B). Moreover, 40 days after weaning the mice off Dox chow, the histology (Figures 5C and 5D) and Mum1 expression pattern (Figures 5E and 5F) of the white pulp of TRE-BPS; CAG-rtTA3 spleens were comparable to controls, confirming that lymphomas had largely regressed.

Braf-rs1 Regulates B-Raf In Vivo

To determine whether *Braf-rs1* functions as a ceRNA for *B-Raf* in vivo, we examined *Braf-rs1*-induced lymphomas for expression of B-Raf and pERK. Notably, *Braf-rs1*-induced lymphomas displayed increased levels of B-Raf and pERK (Figures 5G, 5H, and S4A) compared to adjacent normal white pulp. The difference in B-Raf and pERK levels between tumors and normal white pulp in the same mouse is likely due to positive selection of B cells that express the highest levels of *Braf-rs1*, B-Raf, and pERK.

We next analyzed whether MAPK signaling is critical for the growth of *Braf-rs1*-induced lymphomas. To this end, we treated NSG mice that were transplanted with *Braf-rs1*-induced lymphoma cells with the MEK inhibitor GSK1120212. Notably, treatment with GSK1120212 markedly impaired the ability of transplanted lymphomas to colonize the livers of NSG mice (Figure 5I). Moreover, Dox withdrawal reduced B-Raf and pERK expression in tumors, indicating that increased MAPK activation is stimulated by continuous *Braf-rs1* expression (Figure S4B). These data suggest that *Braf-rs1* elicits its oncogenic effects, at least in part, through B-Raf and the MAPK pathway.

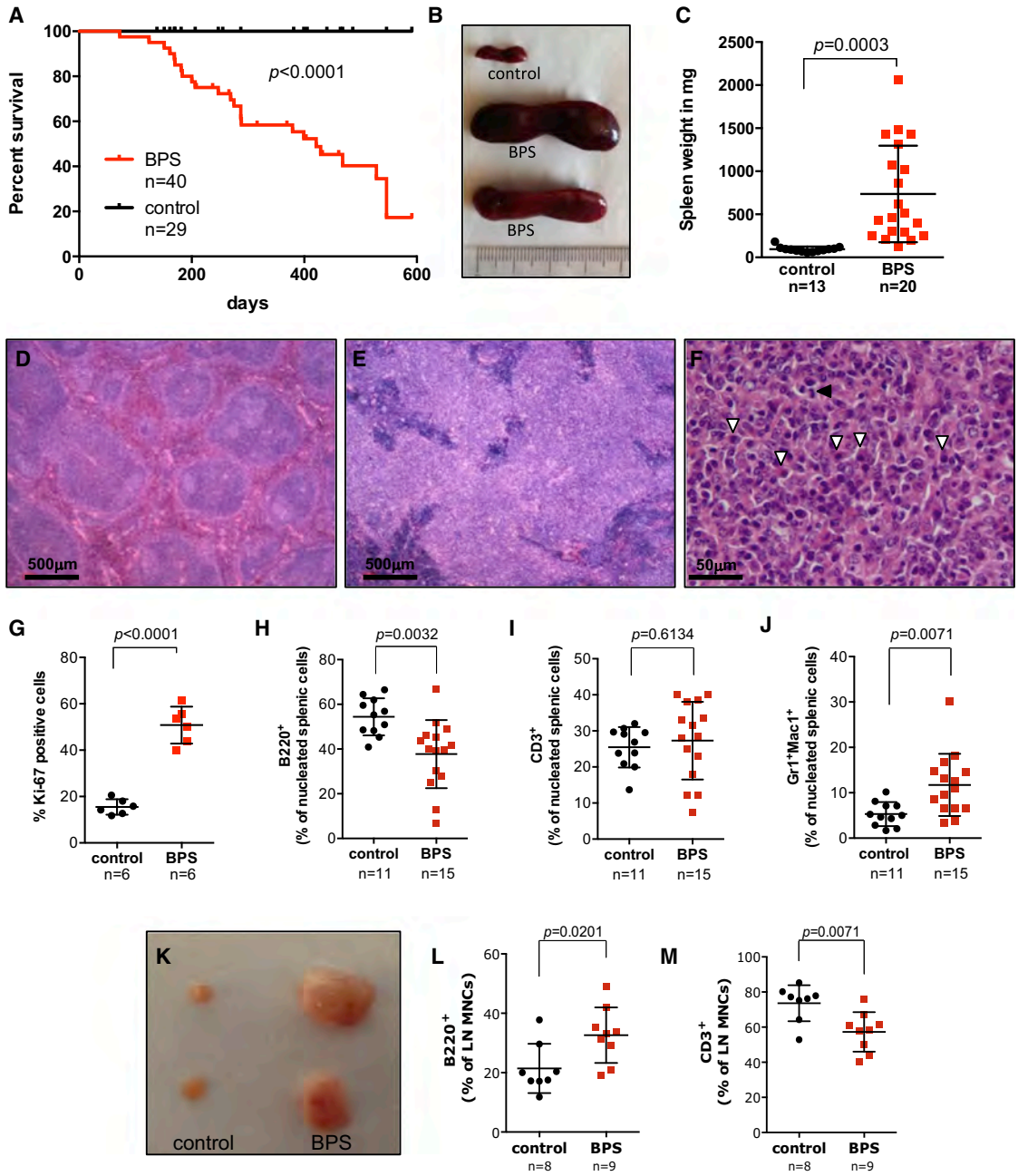

Figure 3. *Braf-rs1* Expression In Vivo Results in a Lymphoid Malignancy

BPS, TRE-BPS; CAG-rtTA3 mice on Dox; control, TRE-BPS, or CAG-rtTA3 mice on Dox here and in all figures.

(A) Survival of BPS and control mice.

(B and C) Size (B) and weight (C) of BPS and control mouse spleens.

(D and E) Photomicrograph of a spleen from a control (D) and BPS mouse (E).

(F) Higher-magnification photomicrograph showing tumor cells in a BPS spleen. White arrowheads denote plasma cells, and black arrowhead highlights a mitotic figure.

(G) Quantification of Ki-67 staining.

(H–J) Flow cytometry-based quantification of splenic B220$^+$ (H), CD3$^+$ (I), and Gr-1$^+$/Mac-1$^+$ (J) populations.

(K) Size of control and BPS mouse lymph nodes.

(L and M) Flow cytometry-based quantification of B220$^+$ (L) and CD3$^+$ (M) populations in lymph nodes.

Error bars represent mean ± SD. See also Figure S3.

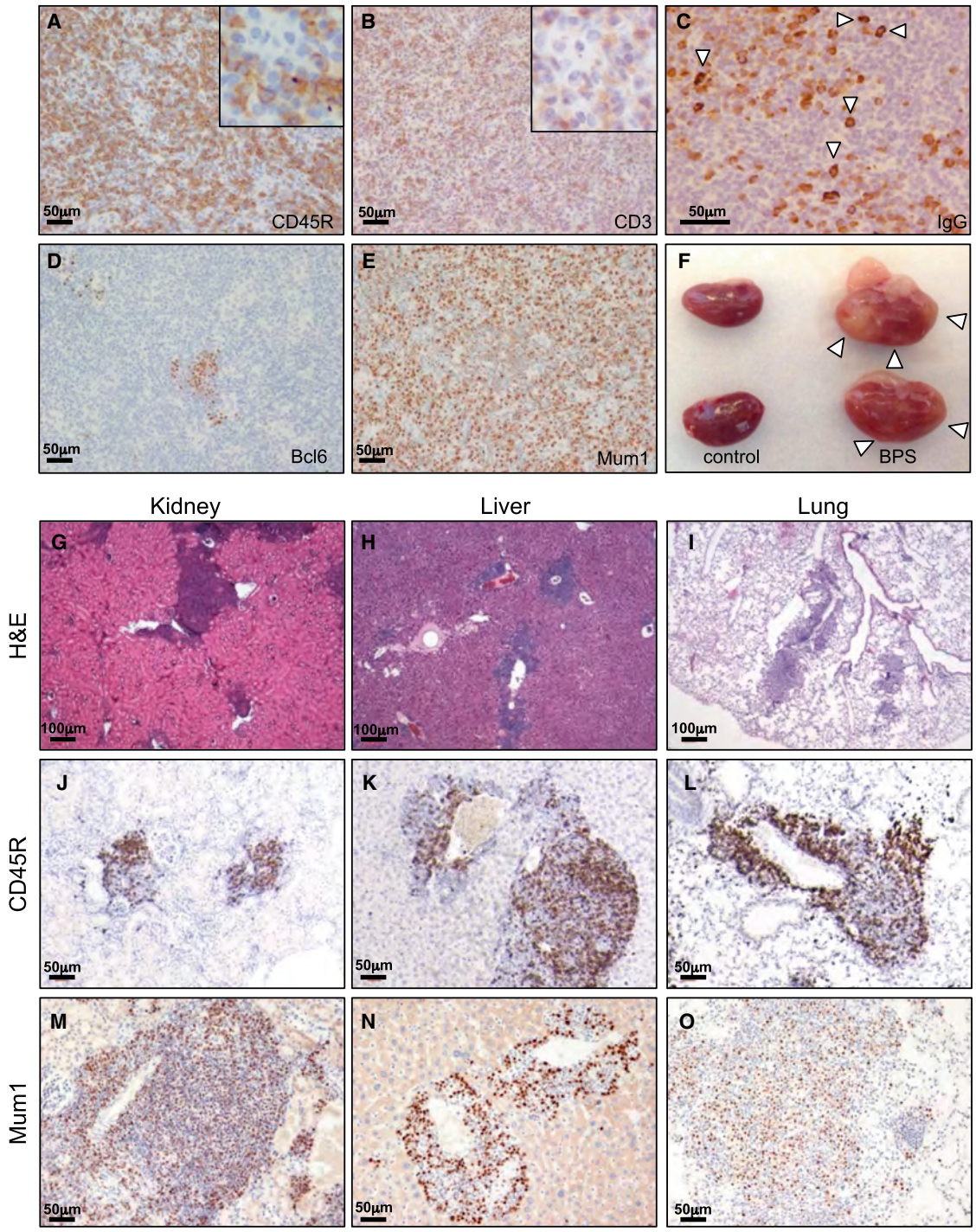

Figure 4. *Braf-rs1* Induces Diffuse Large B Cell Lymphoma

(A) CD45R/B220 staining. Higher magnification inset shows staining of large lymphoma cells.
(B) CD3 staining. Higher-magnification inset shows positive staining of reactive T cells.
(C) IgG staining. Arrowheads denote plasma cells.
(D) Bcl6 staining. Lymphoma cells are negative, and residual germinal center is positive.
(E) Mum1 staining. Tumor cells are positive, and residual germinal center is negative.
(F) Photograph of control and BPS kidneys. Arrowheads denote tumor nodules.
(G–I) H&E staining of kidney (G), liver (H), and lung (I) sections from BPS mice.
(J–L) CD45R/B220 immunohistochemistry of kidney (J), liver (K), and lung (L) sections from BPS mice.
(M–O) Mum1 immunohistochemistry of kidney (M), liver (N), and lung (O) sections from BPS mice.

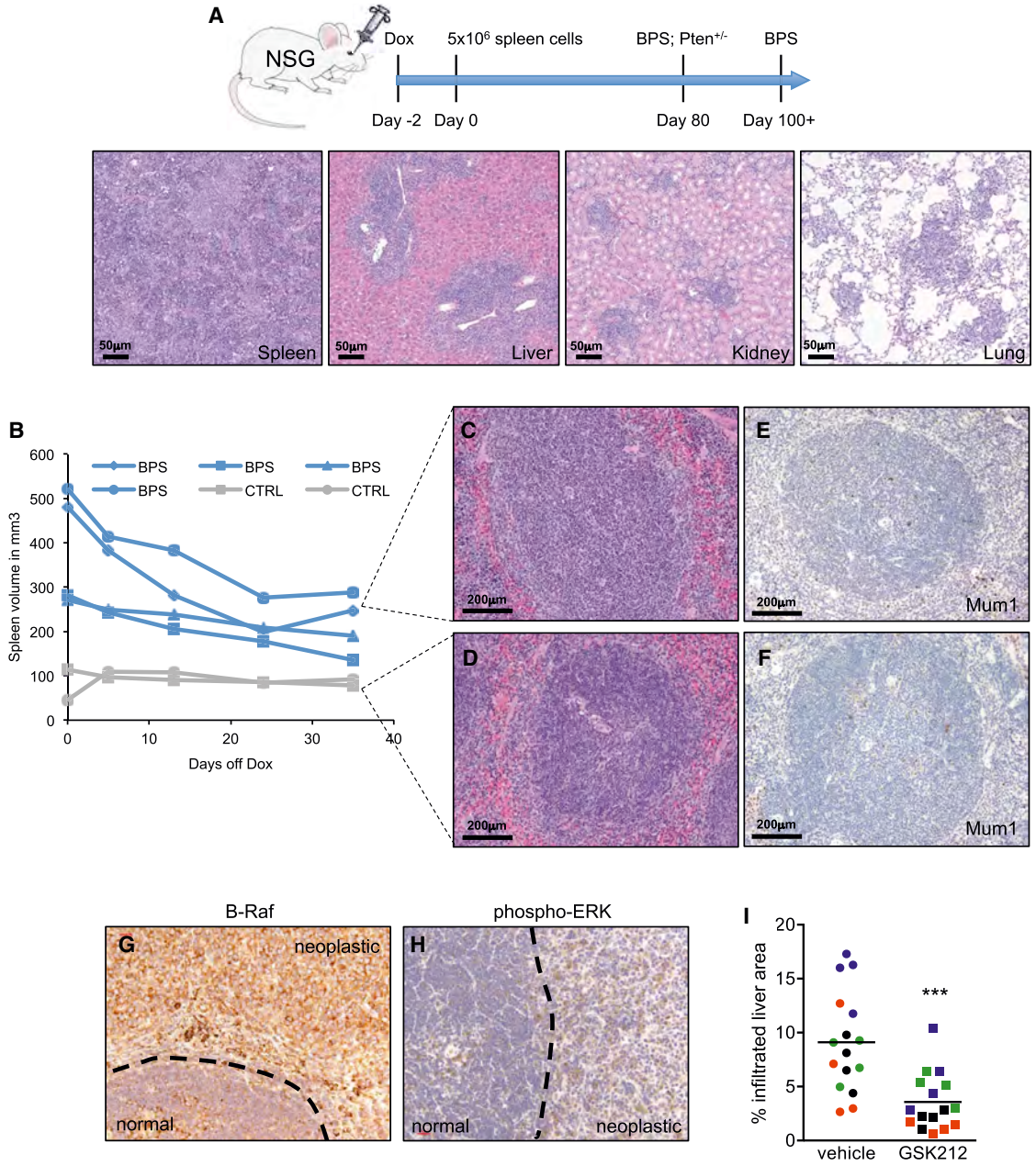

Figure 5. Lymphomas Are Transplantable, Are Addicted to *Braf-rs1* Expression, and Activate the MAPK Pathway

(A) Transplanted lymphoma cells infiltrating the spleen, liver, kidney, and lungs of NSG recipient mice.

(B) Spleen size measurements after Dox withdrawal.

(C–F) H&E staining (C and D) and Mum1 immunohistochemistry (E and F) of BPS and control mouse spleens depicted in (B) after Dox withdrawal.

(G) Immunohistochemical staining for B-Raf of lymphoma and adjacent normal white pulp in BPS spleen.

(H) Immunohistochemical staining for pERK of lymphoma and adjacent normal white pulp in BPS spleen.

(I) Percentage of liver infiltration by TRE-BPS; CAG-rtTA3; Pten$^{+/-}$ lymphoma cells transplanted into NSG mice in response to GSK1120212 treatment. Each symbol represents a liver section, and each recipient mouse is color coded.

Error bars represent mean ± SD. ***p ≤ 0.001. See also Figure S4.

The "CDS" and "3′ UTR" of *Braf-rs1* Possess Oncogenic Potential

Based on *Braf-rs1*'s ability to decoy miRNAs, we reasoned that shorter fragments of *Braf-rs1* may be able to crosstalk with *B-Raf* through a subset of the shared miRNA pool. Such fragments would elicit similar phenotypes provided that the crosstalk remains robust. Alternatively, different portions of *Braf-rs1* may regulate distinct ceRNA networks and yield distinct,

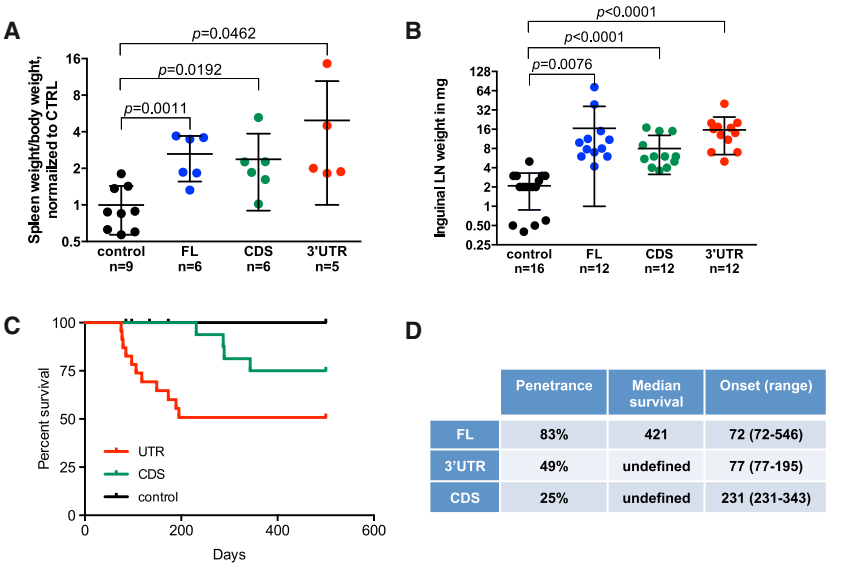

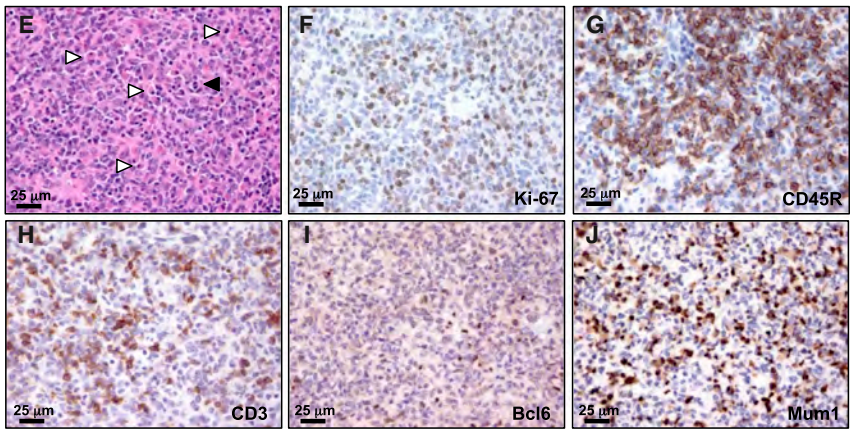

Figure 6. *Braf-rs1*^{CDS} and *Braf-rs1*$^{3'UTR}$ Possess Oncogenic ceRNA Activity Similar to Full-Length *Braf-rs1*

(A and B) Weights of spleens (A) and inguinal lymph nodes (B) of the indicated mouse strains after 6 months on Dox.

(C) Survival of TRE-BPS$^{3'UTR}$ and TRE-BPS^{CDS} mice.

(D) Table summarizing the penetrance, median survival, and disease onset of TRE-BPS, TRE-BPS$^{3'UTR}$, and TRE-BPS^{CDS} mice.

(E) H&E staining of *Braf-rs1*$^{3'UTR}$-induced lymphoma. White arrowheads indicate plasma cells, and black arrowhead indicates mitotic figure.

(F–J) Immunohistochemical staining of *Braf-rs1*$^{3'UTR}$-induced lymphoma for Ki-67 (F), CD45R/B220 (G), CD3 (H), Bcl6 (I), and Mum1 (J).

Error bars represent mean ± SD. See also Figure S5.

B-Raf-unrelated phenotypes. To experimentally examine these possibilities, we generated two additional Dox-inducible mouse models overexpressing either the "CDS" or the "3′ UTR" of *Braf-rs1* (Figures S2C and S2D). TRE-BPS^{CDS} and TRE-BPS$^{3'UTR}$ mice were crossed to CAG-rtTA3 mice and their offspring fed a Dox-containing diet for 6 months. Remarkably, both TRE-BPS^{CDS} and TRE-BPS$^{3'UTR}$ mice displayed enlarged spleens and lymph nodes similar to full-length TRE-BPS mice (Figures 6A and 6B). *Braf-rs1*$^{3'UTR}$ overexpression resulted in splenomegaly and reduced survival (Figures 6C and 6D and S5C) similar to TRE-BPS mice. The histology and immunophenotype of lymphomas in TRE-BPS$^{3'UTR}$ mice were similar to that of full-length TRE-BPS animals (Figures 6E–6J, S5A, and S5B), indicating that *Braf-rs1*$^{3'UTR}$ overexpression elicits a phenotype similar to full-length *Braf-rs1*. TRE-BPS^{CDS} mice developed lymphomas with a reduced penetrance and aggressiveness compared to mice overexpressing full-length *Braf-rs1* or *Braf-rs1*$^{3'UTR}$ (Figures 6C and 6D and data not shown). Similarly, infection of TRE-BPS^{CDS} and TRE-BPS$^{3'UTR}$ MEFs with tTA-pMSCV induced *Braf-rs1*^{CDS} and *Braf-rs1*$^{3'UTR}$ expression (Figure S5D), but only *Braf-rs1*$^{3'UTR}$ elicited a significant effect on B-Raf expression and proliferation, while the *Braf-rs1*^{CDS}-induced effects were negligible (Figures S5D–S5G). *Braf-rs1*^{CDS} and *Braf-rs1*$^{3'UTR}$ may regulate distinct ceRNA networks, but the finding that the severity of the phenotype elicited by the three *Braf-rs1* variants correlated with their ability to deregulate B-Raf provides compelling support to the notion that *Braf-rs1* operates as a proto-oncogenic ceRNA through B-Raf in B cells.

BRAFP1 Is an Oncogenic ceRNA in Human Cancer

Overexpression of human *BRAFP1* increased BRAF and pERK levels as well as proliferation of human cells (Figures 1A, 1D, 1G, and 1H), suggesting that *BRAFP1* may be an oncogene in human cancer. To explore this possibility further, we first determined whether *BRAFP1* is expressed in human DLBCL. Interestingly, *BRAFP1* expression was not found in primary human B cells (Figures 7A and S6A) but was detected in 30% of human primary DLBCL and 20% of human DLBCL cell lines (Figures 7A and S6A). Similar observations have been made in the thyroid, where *BRAFP1* was expressed in some tumors, but not in normal tissue (Zou et al., 2009). Moreover, *BRAFP1* was expressed in melanoma, prostate cancer, and lung cancer cell lines (Figure S6A).

We next interrogated The Cancer Genome Atlas's (TCGA) cBio Cancer Genomics Portal for genomic abnormalities of the locus containing *BRAFP1*. As pseudogene data are not yet included in TCGA, we focused our analysis on two protein-coding genes flanking *BRAFP1*: *ZDHHC15* and *MAGEE2* (Figure S6B). Notably, concurrent copy-number gains and amplification of *ZDHHC15* and *MAGEE2* were observed in numerous cancer types (Figure S6B). Importantly, *BRAFP1* expression could be detected in such cancer types (Kalyana-Sundaram et al., 2012). Thus, both transcriptional mechanisms and genomic

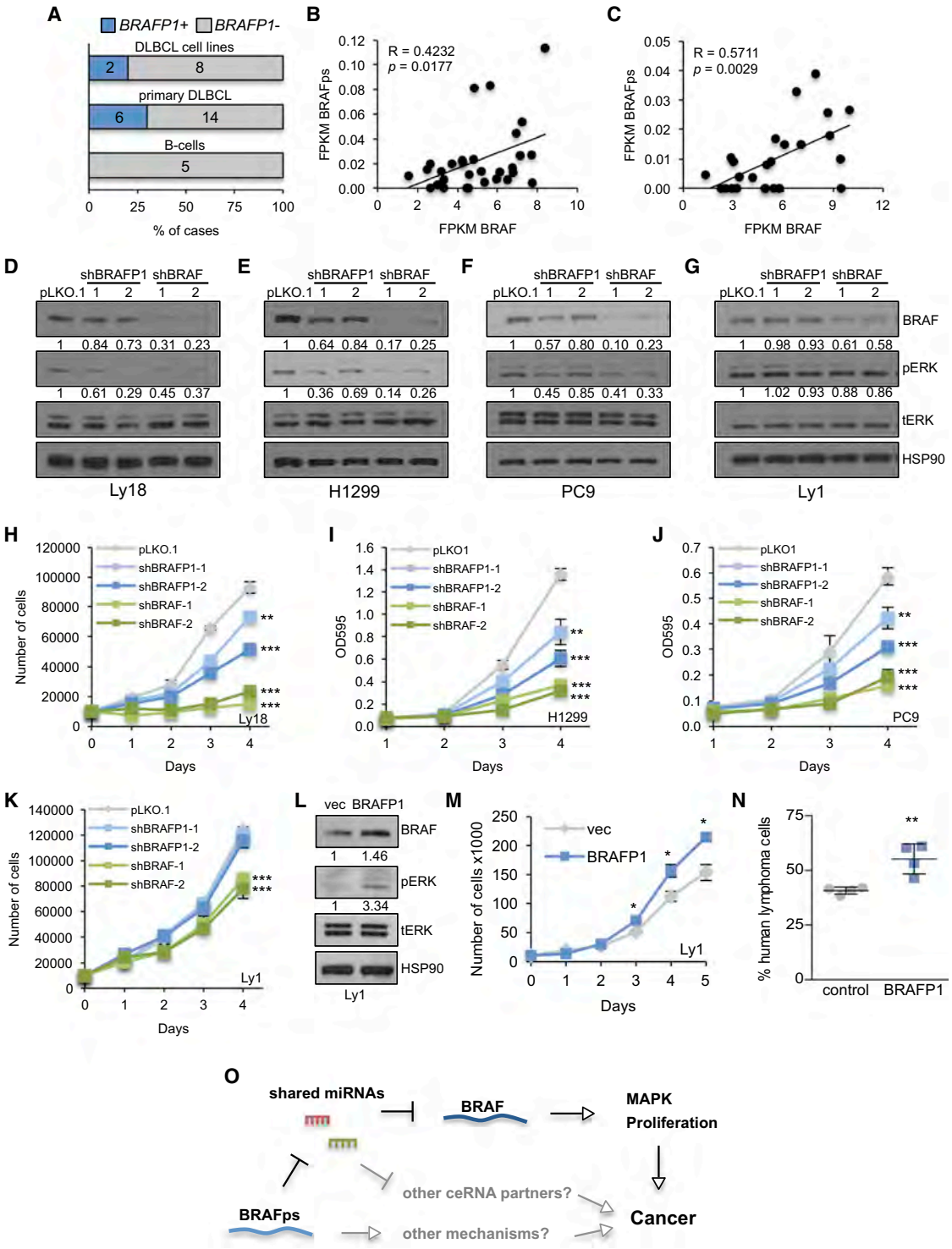

Figure 7. *BRAFP1* in Human Cancer

(A) Percentage of primary human B cells, primary human DLBCL, and human DLBCL cell lines expressing *BRAFP1* as determined by qPCR analysis.

(B and C) Positive correlation of *BRAFP1* and *BRAF* expression in human DLBCL primary tumors (B) and cell lines (C).

(D–G) Western blot for BRAF and pERK in OCI-Ly18 (D), H1299 (E), PC9 (F), and OCI-Ly1 (G) cells in response to *BRAFP1* silencing.

(H–K) Proliferation of OCI-Ly18 (H), H1299 (I), PC9 (J), and OCI-Ly1 (K) cells in response to *BRAFP1* silencing.

(L) Western blot for BRAF and pERK in OCI-Ly1 cells overexpressing *BRAFP1*.

(legend continued on next page)

aberrations may lead to abnormal *BRAFP1* expression in human cancer.

Our experiments in human cell lines indicate that *BRAFP1* may operate as a ceRNA to regulate BRAF expression. Accordingly, analysis of RNA sequencing data revealed that *BRAFP1* and *BRAF* expression were positively correlated in primary human DLBCL tumors and DLBCL cell lines (Figure 7B and 7C). We also analyzed whether the expression of dual-targeting miRNAs correlates with *BRAF* and/or *BRAFP1* expression. While miR-590 expression negatively correlated with *BRAFP1* levels, miR-30a, miR-182, and miR-876 showed no correlation (Figure S6C). Thus, similar to our observations in TRE-BPS MEFs, expression of *BRAFP1* and *BRAF* may not affect miRNA abundance in human DLBCL.

To functionally validate the oncogenic function of *BRAFP1* in human cancer, we designed shRNAs to specifically silence expression of endogenous *BRAFP1* (Figure S6H). Knockdown of *BRAFP1* in OCI-Ly18 DLBCL cells and H1299 and PC9 lung cancer cells reduced the expression of BRAF and pERK (Figures 7D–7F and S6I–S6K). *BRAFP1* silencing moderately reduced *BRAF* mRNA levels in OCI-Ly18 and PC9 cells, but not in H1299 cells, suggesting that the mechanism of miRNA-mediated regulation of *BRAF* varies between cell lines. Importantly, the *BRAFP1* hairpins had no effect on BRAF and pERK expression in OCI-Ly1 DLBCL cells that do not express endogenous *BRAFP1* (Figure 7G). Moreover, *BRAFP1* silencing reduced proliferation of OCI-Ly18, H1299, and PC9 cells, but not of OCI-Ly1 cells (Figures 7H–7K). Remarkably, silencing of endogenous *BRAFP1* elicited a significant effect on BRAF expression in OCI-Ly18, H1299, and PC9 cells even though it is ~15- to ~30-fold less abundant than *BRAF* (Figures S6D and S6E). Intriguingly, *BRAFp1* was turned over significantly faster than *BRAF* (Figure S6F), suggesting that the relatively low expression levels of *BRAFP1* may be due to its short half-life. We also determined the abundance of miR-30a, miR-182, and miR-876 in OCI-Ly18, H1299, and PC9 cells and found that their expression levels were in the same range as those of *BRAFP1* and *BRAF* (Figures S6G).

Overexpression of *BRAFP1* in three human DLBCL cell lines lacking endogenous *BRAFP1* expression, SU-DHL-4, Karpas422, and OCI-Ly1 (Figures S6A and S6L), resulted in elevated BRAF and pERK levels (Figures 7L and S6M). Moreover, *BRAFP1* overexpression increased proliferation of all three DLBCL cell lines (Figures 7M, S6N, and S6O) and resulted in increased growth of xenotransplanted OCI-Ly1 cells in the bone marrow of NSG recipients (Figure 7N). These data suggest that *BRAFP1* has oncogenic properties in human cancer.

DISCUSSION

We investigated whether pseudogenes exert critical functions in the context of a whole organism and whether their perturbation contributes to the development of disease. We focused on the *BRAF* pseudogene, as it exists in humans and mice and is deregulated in cancer (Kalyana-Sundaram et al., 2012; Zou et al., 2009). Our study establishes the *BRAF* pseudogene as a potent proto-oncogene that can elicit a phenotype resembling human diffuse large B cell lymphoma. Remarkably, no additional engineered mutations were required to drive this phenotype, and lymphomas completely regressed upon Dox withdrawal, emphasizing the oncogenic potential of the *BRAF* pseudogene. While it is possible that the *BRAF* pseudogene elicits its effects through more than one mechanism or pathway, the fact that both the CDS and the 3′ UTR of *Braf-rs1* displayed a similar phenotype to full-length *Braf-rs1*, albeit with different severity, supports the notion that *Braf-rs1* functions as a ceRNA to regulate B-Raf in vivo (Figure 7O). Whether the oncogenic activity of *Braf-rs1* also requires additional ceRNA targets or non-ceRNA-related mechanisms will be the focus of future studies.

Several groups, including ours, have generated mathematical models to quantitatively assess the response of a ceRNA network to perturbations (Ala et al., 2013; Bosia et al., 2013; Figliuzzi et al., 2013). More recently, such models were used in conjunction with miRNA predictions, RNA sequencing, and target site occupancy analyses to more accurately characterize miRNA competition (Bosson et al., 2014; Denzler et al., 2014; Jens and Rajewsky, 2014). Intriguingly, these studies yielded disparate conclusions. It was proposed that ceRNA crosstalk is unlikely to occur upon physiological changes of ceRNA expression based on these models' estimates of the number of additional target sites required to achieve significant expression changes of other targets (Denzler et al., 2014; Jens and Rajewsky, 2014). By contrast, using Argonaute iCLIP and RNA-seq, Sharp and colleagues determined that a relatively low number of additional target sites could elicit ceRNA crosstalk when the number of miRNA molecules and high-affinity target sites approaches equimolarity (Bosson et al., 2014). Interestingly, *BRAFP1* is several-fold less abundant than *BRAF*, yet its silencing significantly diminished BRAF expression levels, MAPK signaling, and proliferation. *BRAF* and its pseudogene harbor high-affinity sites for the murine and human miRNAs that we validated as potential mediators of the ceRNA crosstalk (miRs-134, -543, and -653 and miRs-30a, -182, -876, respectively). Notably, the levels of these miRNAs in mouse spleens and lymphomas as well as human cancer cell lines are amenable to miRNA competition in accordance with the model proposed by Bosson et al. Thus, a ceRNA effect of *BRAFP1* that is solely based on miRNA competition may be compatible with this model.

Importantly, the studies by the groups of Sharp, Stoffel, and Rajewsky focused on ceRNA regulation that is mediated by a single miRNA. However, ceRNA pairs in general, and gene/pseudogene pairs in particular, share numerous miRNAs. This increases the likelihood of shared miRNAs being present at crosstalk-favoring levels, and we have shown that ceRNA crosstalk is enhanced when it is mediated by more miRNAs (Ala et al., 2013).

(M) Proliferation of OCI-Ly1 cells.

(N) Percentage of human $CD19^+$ transplanted OCI-Ly1 cells in bone marrow of NSG recipients.

(O) Model depicting the proposed oncogenic action of the *BRAF* pseudogene.

Error bars represent mean ± SD. *$p \leq 0.05$; **$p \leq 0.01$; ***$p \leq 0.001$. See also Figure S6.

As discussed by Jens and Rajewsky, several factors that may influence ceRNA crosstalk are neglected in current mathematical models. For instance, subcellular co-localization of miRNAs and competing targets may result in local concentrations that favor ceRNA crosstalk. In addition, target degradation may trap miRNAs in P bodies or other sites of RNA decay, thus amplifying the ceRNA regulation by removing miRNAs from the available pool. Intriguingly, *BRAFP1* is degraded significantly faster than *BRAF* (Figure S6F); however, whether this influences the ceRNA activity of *BRAFP1* remains to be determined. Future improvements to both quantitative measurements and mathematical models will undoubtedly provide a better understanding of the molecular conditions required for ceRNA crosstalk. However, it should be noted that ceRNA crosstalk can be predicted solely based on the MRE overlap of transcripts (Chiu et al., 2014; Karreth et al., 2011; Sumazin et al., 2011; Tay et al., 2011), suggesting that miRNA competition is indeed the central component of ceRNA crosstalk.

Human hematopoietic malignancies are associated with "overdosage" of the X chromosome, which harbors the *BRAF* pseudogene locus. This can occur through *XIST* deletion and X chromosome duplication in women with myeloid cancers, and extra X chromosomes have been noted in a variety of hematopoietic cancers of both sexes (Dewald et al., 1989; Dierlamm et al., 1995; Heinonen et al., 1999; Paulsson et al., 2010; Rack et al., 1994; Yamamoto et al., 2002), including DLBCL (Bea et al., 2005; Monni et al., 1996; Morin et al., 2013). Our analysis revealed that a variety of human cancers harbor copy-number gains and amplifications of the locus containing *BRAFP1*. It is therefore tempting to speculate that increased X dosage and the potentially associated overexpression of *BRAFP1* contribute to the development and/or progression of cancer cases harboring more than one active copy of the X chromosome. Moreover, elevated expression of *BRAFP1* has been observed in cancers other than DLBCL (Kalyana-Sundaram et al., 2012; Zou et al., 2009), and transcriptional deregulation may thus be another means to deregulate *BRAFP1* expression. Whether *BRAFP1* has oncogenic potential in other organs such as the thyroid remains to be determined through the use of tissue-specific overexpression of the BRAF pseudogene.

Interestingly, several observations suggest that the *BRAF* pseudogenes evolved independently in mice and humans. First, they reside in non-syngeneic locations—on chromosome 10 in mice and on the X chromosome in humans. Second, the 3′ UTR of the *BRAF* gene is not conserved between mice and humans; importantly, however, the *BRAF* pseudogene 3′ UTRs display high sequence homology to their parental counterparts in the respective species. Third, murine *Braf-rs1* arose from an alternative *B-Raf* splice form that is specific to mice (Karreth et al., 2009). The likely parallel yet converging evolution of *BRAFP1* and *Braf-rs1* and the fact that the gene-pseudogene crosstalk is mediated by different miRNAs in the two species suggest that their functions may be conserved. Indeed, the frequent *BRAFP1* copy-number gains and transcriptional activation of *BRAFP1* in human cancers as well as our silencing and overexpression experiments indicate that our findings in the mouse are of relevance to human disease.

It was recently proposed that human *BRAFP1* encodes a peptide with the ability to activate the MAPK pathway (Zou et al., 2009). We neither detected any peptide translation by the mouse or human *BRAF* pseudogenes nor could we detect robust association of *Braf-rs1* with actively translating ribosomes (data not shown). These findings suggest that *Braf-rs1* is not translated into an oncogenic peptide but, rather, exerts its function as a RNA transcript. This is further supported by the finding that TRE-BPS$^{3'UTR}$ mice display a more severe phenotype compared to TRE-BPS^{CDS} mice, which suggests that the effects of *Braf-rs1* on *B-Raf* are primarily mediated through its 3′ UTR. The *BRAFP1* ORF predicted by Zou et al., however, localizes to the CDS portion of the pseudogene.

Pseudogenes were considered genomic junk for decades, but their retention during evolution argues that they may possess important functions and that their deregulation could contribute to the development of disease. Indeed, several lines of evidence have associated pseudogenes with cellular transformation (Poliseno, 2012). Our study shows that aberrant expression of a pseudogene causes cancer, thus vastly expanding the number of genes that may be involved in this disease. Moreover, our work emphasizes the functional importance of the non-coding dimension of the transcriptome and should stimulate further studies of the role of pseudogenes in the development of disease.

EXPERIMENTAL PROCEDURES

Flow Cytometry

Mice were euthanized and single-cell suspensions from spleens and lymph nodes were prepared by passing organs through 100 μm cell strainers in 2% FBS/PBS, centrifuged and re-suspended in 1–2 ml ACK red cell lysis buffer (GIBCO). Red blood cells were lysed on ice for 1 min. Cell suspensions were then washed in 2% FBS/PBS, centrifuged and re-suspended in 1 ml 2% FBS/PBS. For hematopoietic lineage analysis, we used monoclonal antibodies specific for the following: CD3e-PE (145-2C11), B220-FITC (RA3-6B2), Gr-1-APC (RB6-8C5), and CD11b-PE/Cy7 (M1/70). All antibodies were from eBioscience. To assess cell viability, cells were incubated with DAPI prior to FACS analysis. All staining mixtures were analyzed on a BD LSR II flow cytometer (Becton Dickinson). Resulting profiles were further processed and analyzed using the FlowJo 8.7 software. For fold change quantifications, both mutant and control cell populations were normalized to the average of the controls. At least five mice from different litters were used for all flow cytometry experiments.

Tissue Fixation, H&E, and IHC

Tissues were fixed in 4% paraformaldehyde overnight and embedded in paraffin according to standard procedures. 5 μm sections were either stained with hematoxylin & eosin or with the following antibodies: CD45R/B220 (ab64100, Abcam), CD3 (ab5690, Abcam), Ki-67 (RM-9106-S1, Thermo Scientific), IgG (BA2000, Vector), BRAF (sc-9002, Santa Cruz), pERK (4373, Cell Signaling), Bcl-6 (5650, Cell Signaling), and Mum1 (sc-6059, Santa Cruz). Organs from at least five mice from different litters were used for all stainings.

Cell Culture

HCT116 and HeLa were from ATCC, Dicer mutant HCT116 cells were provided by B. Vogelstein, and *Dicer*$^{FL/\Delta}$ and *Dicer*$^{\Delta/\Delta}$ mouse sarcoma cells were provided by P. Sharp and were cultured in DMEM containing 10% FCS and 2 mM L-glutamine. PC9, H1299, H441, and H2009 (all provided by L. Cantley), OCI-Ly8, OCI-Ly3, RCK8, and Val were grown in RPMI-1640 containing 10% FCS and 2 mM L-glutamine. SU-DHL-4, SU-DHL-8, Karpas422, OCI-Ly7, Toledo, OCI-Ly1, and OCI-Ly18 cells were grown as previously described

(Chapuy et al., 2013). Cells were regularly tested with MycoAlert (Lonza) to ascertain that cells were not infected with mycoplasma.

Plasmids, Transfection, and Virus Infection

Human *BRAFP1* was cloned into pLenti-CMV-GFP-Puro (Addgene 25873) and pCDNA3, and mouse *Braf-rs1* was cloned into pCCL.sin.PPT.hPGK.GFP.Wpre (L277, L. Naldini) or pCDNA3-neo. pMSCV-tTA (Addgene #18783) was used to induce *Braf-rs1* expression in TRE-BPS MEFs. Lipofectamine 2000 was used for plasmid transfection. Lentivirus or retrovirus was produced in HEK293T LentiX cells (Clontech) co-transfected with VSVG, pMDL, and Rev or Eco helper plasmids, respectively. Viral supernatants were filtered and cells infected in the presence of 5 μg/ml polybrene.

Proliferation Assays

For proliferation assays, 2×10^4 cells were plated in four 12-well plates in triplicates. Every day, one plate was fixed with 4% paraformaldehyde and stained with Crystal Violet. The dye was extracted with 10% acetic acid and its absorbance determined at OD_{595}. For suspension cells, 1×10^4 cells were plated in triplicates in round-bottom 96-well plates and counted every day for 5 days.

Luciferase Assays

HCT116 cells were transfected with 150 ng of psiCHECK2 vector or psiCHECK2-humanBRAF 3′ UTR and 1 mg human *BRAFP1* constructs using Lipofectamine 2000. To validate miRNA targeting, 3′ UTRs of murine and human gene and pseudogene were cloned into psiCHECK2. 5×10^4 HEK293T cells were transfected in 48-well plates with 20 ng of psiCHECK2 reporter and 100 nM miRNA mimic (QIAGEN). To test the ceRNA activity of the *BRAF* pseudogenes, 5×10^4 HEK293T cells were transfected in 48-well plates with 20 ng of psiCHECK2 reporter and 250 ng of murine Braf-rs1-L277 vector or human BRFAP1-pCDNA3 and 1–2 nM miRNA mimic. In all transfections, firefly luciferase activity was used as a normalization control for transfection efficiency. 48 hr after transfection, luciferase activities were measured consecutively with the dual luciferase reporter system (Promega).

Western Blot

Cells were lysed in RIPA buffer containing HALT protease and phosphatase inhibitors (Sigma). 20 μg total protein were separated on 4%–12% Bis-Tris acrylamide NuPAGE gradient gels in MOPS SDS buffer (Invitrogen). The following antibodies were used: HSP90 (610419, BD), BRAF (sc5284, Santa Cruz), pERK (9101, Cell Signaling), and tERK (9102, Cell Signaling). Secondary HRP-tagged antibodies and ECL detection reagent were from Amersham. Image J software was used for quantification.

SUPPLEMENTAL INFORMATION

Supplemental Information includes Extended Experimental Procedures, six figures, and two tables and can be found with this article online at http://dx.doi.org/10.1016/j.cell.2015.02.043.

AUTHOR CONTRIBUTIONS

F.A.K. and P.P.P. conceived and designed the study. F.A.K., M.R., A.R., Y.T., D.W., N.S., and A.B. performed experiments, and F.A.K., M.R., and P.P.P. analyzed most data. C.N., J.F., and F.L. carried out immunohistochemistry. U.A. performed miRNA predictions. R.C. and S.J.R. evaluated histopathology of tumors and advised on immunohistochemical validation. M.S., T.M.K., M.D.C.V.-H., and D.J.A. performed RNA-seq analysis. B.C. and M.A.S. provided human samples and cell lines. A.V. and O.E. analyzed *BRAFP1* expression in human RNA-seq data. F.A.K. and P.P.P. wrote the manuscript with contributions from all authors.

ACKNOWLEDGMENTS

We are grateful to L. Cantley for hosting F.A.K. in his lab for part of this study. We thank S. Lowe for CAG-rtTA3 mice; L. Cantley, B. Vogelstein, and P. Sharp for cell lines; G. DeNicola for helpful discussions; and the Nikon Imaging Center at Harvard Medical School for help with light microscopy, the Dana Farber/Harvard Cancer Center Specialized Histopathology Core for help with immunohistochemistry, J. Clohessy and B. Padmani for help with ultrasound imaging, and S. Annunziato, A. Nyein, A. Bester, and K Berry for technical assistance. F.A.K. was supported by fellowships from the Department of Defense Prostate Cancer Research Program and the American Cancer Society. M.R. was supported by the German Academy of Sciences Leopoldina, F.L. received a CHB-MIT fellowship, and U.A. acknowledges support from the Italian Association for Cancer Research (AIRC) under grant IG-9408. M.S., T.M.K., M.D.C.V.-H., and D.J.A. are funded by Cancer Research UK and the Wellcome Trust. R.C. was supported by a FP7 ERC-2009-StG grant (Proposal No. 242965, "Lunely"), AIRC grant IG-12023, and an International Association for Cancer Research (AICR) grant 12-0216. P.P.P. was supported by NIH grant CA170158-01.

Received: August 26, 2014
Revised: December 19, 2014
Accepted: February 2, 2015
Published: April 2, 2015

REFERENCES

Ala, U., Karreth, F.A., Bosia, C., Pagnani, A., Taulli, R., Léopold, V., Tay, Y., Provero, P., Zecchina, R., and Pandolfi, P.P. (2013). Integrated transcriptional and competitive endogenous RNA networks are cross-regulated in permissive molecular environments. Proc. Natl. Acad. Sci. USA *110*, 7154–7159.

Bea, S., Zettl, A., Wright, G., Salaverria, I., Jehn, P., Moreno, V., Burek, C., Ott, G., Puig, X., Yang, L., et al.; Lymphoma/Leukemia Molecular Profiling Project (2005). Diffuse large B-cell lymphoma subgroups have distinct genetic profiles that influence tumor biology and improve gene-expression-based survival prediction. Blood *106*, 3183–3190.

Beard, C., Hochedlinger, K., Plath, K., Wutz, A., and Jaenisch, R. (2006). Efficient method to generate single-copy transgenic mice by site-specific integration in embryonic stem cells. Genesis *44*, 23–28.

Bier, A., Oviedo-Landaverde, I., Zhao, J., Mamane, Y., Kandouz, M., and Batist, G. (2009). Connexin43 pseudogene in breast cancer cells offers a novel therapeutic target. Mol. Cancer Ther. *8*, 786–793.

Bosia, C., Pagnani, A., and Zecchina, R. (2013). Modelling Competing Endogenous RNA Networks. PLoS ONE *8*, e66609.

Bosson, A.D., Zamudio, J.R., and Sharp, P.A. (2014). Endogenous miRNA and target concentrations determine susceptibility to potential ceRNA competition. Mol. Cell *56*, 347–359.

Cazalla, D., Yario, T., and Steitz, J.A. (2010). Down-regulation of a host microRNA by a Herpesvirus saimiri noncoding RNA. Science *328*, 1563–1566.

Cesana, M., Cacchiarelli, D., Legnini, I., Santini, T., Sthandier, O., Chinappi, M., Tramontano, A., and Bozzoni, I. (2011). A long noncoding RNA controls muscle differentiation by functioning as a competing endogenous RNA. Cell *147*, 358–369.

Chapuy, B., McKeown, M.R., Lin, C.Y., Monti, S., Roemer, M.G.M., Qi, J., Rahl, P.B., Sun, H.H., Yeda, K.T., Doench, J.G., et al. (2013). Discovery and characterization of super-enhancer-associated dependencies in diffuse large B cell lymphoma. Cancer Cell *24*, 777–790.

Chiefari, E., Iiritano, S., Paonessa, F., Le Pera, I., Arcidiacono, B., Filocamo, M., Foti, D., Liebhaber, S.A., and Brunetti, A. (2010). Pseudogene-mediated posttranscriptional silencing of HMGA1 can result in insulin resistance and type 2 diabetes. Nat. Commun. *1*, 40–47.

Chiu, H.-S., Llobet-Navas, D., Yang, X., Chung, W.-J., Ambesi-Impiombato, A., Iyer, A., Kim, H.R., Seviour, E.G., Luo, Z., Sehgal, V., et al. (2014). Cupid: simultaneous reconstruction of microRNA-target and ceRNA networks. Genome Res. *25*, 257–267.

Cummins, J.M., He, Y., Leary, R.J., Pagliarini, R., Diaz, L.A., Jr., Sjoblom, T., Barad, O., Bentwich, Z., Szafranska, A.E., Labourier, E., et al. (2006). The colorectal microRNAome. Proc. Natl. Acad. Sci. USA *103*, 3687–3692.

Denzler, R., Agarwal, V., Stefano, J., Bartel, D.P., and Stoffel, M. (2014). Assessing the ceRNA hypothesis with quantitative measurements of miRNA and target abundance. Mol. Cell *54*, 766–776.

Dewald, G.W., Brecher, M., Travis, L.B., and Stupca, P.J. (1989). Twenty-six patients with hematologic disorders and X chromosome abnormalities. Frequent idic(X)(q13) chromosomes and Xq13 anomalies associated with pathologic ringed sideroblasts. Cancer Genet. Cytogenet. *42*, 173–185.

Dierlamm, J., Michaux, L., Criel, A., Wlodarska, I., Zeller, W., Louwagie, A., Michaux, J.L., Mecucci, C., and Van den Berghe, H. (1995). Isodicentric (X)(q13) in haematological malignancies: presentation of five new cases, application of fluorescence in situ hybridization (FISH) and review of the literature. Br. J. Haematol. *91*, 885–891.

Figliuzzi, M., Marinari, E., and De Martino, A. (2013). MicroRNAs as a selective channel of communication between competing RNAs: a steady-state theory. Biophys. J. *104*, 1203–1213.

Franco-Zorrilla, J.M., Valli, A., Todesco, M., Mateos, I., Puga, M.I., Rubio-Somoza, I., Leyva, A., Weigel, D., García, J.A., and Paz-Ares, J. (2007). Target mimicry provides a new mechanism for regulation of microRNA activity. Nat. Genet. *39*, 1033–1037.

Gutschner, T., and Diederichs, S. (2012). The hallmarks of cancer: a long non-coding RNA point of view. RNA Biol. *9*, 703–719.

Han, Y.J., Ma, S.F., Yourek, G., Park, Y.-D., and Garcia, J.G.N. (2011). A transcribed pseudogene of MYLK promotes cell proliferation. FASEB J. *25*, 2305–2312.

Hansen, T.B., Jensen, T.I., Clausen, B.H., Bramsen, J.B., Finsen, B., Damgaard, C.K., and Kjems, J. (2013). Natural RNA circles function as efficient microRNA sponges. Nature *495*, 384–388.

Hawkins, P.G., and Morris, K.V. (2010). Transcriptional regulation of Oct4 by a long non-coding RNA antisense to Oct4-pseudogene 5. Transcription *1*, 165–175.

Heinonen, K., Mahlamäki, E., Riikonen, P., Meltoranta, R.L., Rahiala, J., and Perkkiö, M. (1999). Acquired X-chromosome aneuploidy in children with acute lymphoblastic leukemia. Med. Pediatr. Oncol. *32*, 360–365.

Jens, M., and Rajewsky, N. (2014). Competition between target sites of regulators shapes post-transcriptional gene regulation. Nat. Rev. Genet. *16*, 113–126.

Johnsson, P., Ackley, A., Vidarsdottir, L., Lui, W.-O., Corcoran, M., Grandér, D., and Morris, K.V. (2013). A pseudogene long-noncoding-RNA network regulates PTEN transcription and translation in human cells. Nat. Struct. Mol. Biol. *20*, 440–446.

Kalyana-Sundaram, S., Kumar-Sinha, C., Shankar, S., Robinson, D.R., Wu, Y.-M., Cao, X., Asangani, I.A., Kothari, V., Prensner, J.R., Lonigro, R.J., et al. (2012). Expressed pseudogenes in the transcriptional landscape of human cancers. Cell *149*, 1622–1634.

Karreth, F.A., DeNicola, G.M., Winter, S.P., and Tuveson, D.A. (2009). C-Raf inhibits MAPK activation and transformation by B-Raf(V600E). Mol. Cell *36*, 477–486.

Karreth, F.A., Tay, Y., Perna, D., Ala, U., Tan, S.M., Rust, A.G., DeNicola, G., Webster, K.A., Weiss, D., Perez-Mancera, P.A., et al. (2011). In vivo identification of tumor- suppressive PTEN ceRNAs in an oncogenic BRAF-induced mouse model of melanoma. Cell *147*, 382–395.

Libri, V., Helwak, A., Miesen, P., Santhakumar, D., Borger, J.G., Kudla, G., Grey, F., Tollervey, D., and Buck, A.H. (2012). Murine cytomegalovirus encodes a miR-27 inhibitor disguised as a target. Proc. Natl. Acad. Sci. USA *109*, 279–284.

Marcinowski, L., Tanguy, M., Krmpotic, A., Rädle, B., Lisnić, V.J., Tuddenham, L., Chane-Woon-Ming, B., Ruzsics, Z., Erhard, F., Benkartek, C., et al. (2012). Degradation of cellular mir-27 by a novel, highly abundant viral transcript is important for efficient virus replication in vivo. PLoS Pathog. *8*, e1002510.

Memczak, S., Jens, M., Elefsinioti, A., Torti, F., Krueger, J., Rybak, A., Maier, L., Mackowiak, S.D., Gregersen, L.H., Munschauer, M., et al. (2013). Circular RNAs are a large class of animal RNAs with regulatory potency. Nature *495*, 333–338.

Monni, O., Joensuu, H., Franssila, K., and Knuutila, S. (1996). DNA copy number changes in diffuse large B-cell lymphoma—comparative genomic hybridization study. Blood *87*, 5269–5278.

Morin, R.D., Mungall, K., Pleasance, E., Mungall, A.J., Goya, R., Huff, R.D., Scott, D.W., Ding, J., Roth, A., Chiu, R., et al. (2013). Mutational and structural analysis of diffuse large B-cell lymphoma using whole-genome sequencing. Blood *122*, 1256–1265.

Paulsson, K., Haferlach, C., Fonatsch, C., Hagemeijer, A., Andersen, M.K., Slovak, M.L., and Johansson, B.; MDS Foundation (2010). The idic(X)(q13) in myeloid malignancies: breakpoint clustering in segmental duplications and association with TET2 mutations. Hum. Mol. Genet. *19*, 1507–1514.

Poliseno, L. (2012). Pseudogenes: newly discovered players in human cancer. Sci. Signal. *5*, re5.

Poliseno, L., Salmena, L., Zhang, J., Carver, B., Haveman, W.J., and Pandolfi, P.P. (2010). A coding-independent function of gene and pseudogene mRNAs regulates tumour biology. Nature *465*, 1033–1038.

Premsrirut, P.K., Dow, L.E., Kim, S.Y., Camiolo, M., Malone, C.D., Miething, C., Scuoppo, C., Zuber, J., Dickins, R.A., Kogan, S.C., et al. (2011). A rapid and scalable system for studying gene function in mice using conditional RNA interference. Cell *145*, 145–158.

Rack, K.A., Chelly, J., Gibbons, R.J., Rider, S., Benjamin, D., Lafreniére, R.G., Oscier, D., Hendriks, R.W., Craig, I.W., Willard, H.F., et al. (1994). Absence of the XIST gene from late-replicating isodicentric X chromosomes in leukaemia. Hum. Mol. Genet. *3*, 1053–1059.

Ravi, A., Gurtan, A.M., Kumar, M.S., Bhutkar, A., Chin, C., Lu, V., Lees, J.A., Jacks, T., and Sharp, P.A. (2012). Proliferation and tumorigenesis of a murine sarcoma cell line in the absence of DICER1. Cancer Cell *21*, 848–855.

Salmena, L., Poliseno, L., Tay, Y., Kats, L., and Pandolfi, P.P. (2011). A ceRNA hypothesis: the Rosetta Stone of a hidden RNA language? Cell *146*, 353–358.

Sumazin, P., Yang, X., Chiu, H.-S., Chung, W.-J., Iyer, A., Llobet-Navas, D., Rajbhandari, P., Bansal, M., Guarnieri, P., Silva, J., and Califano, A. (2011). An extensive microRNA-mediated network of RNA-RNA interactions regulates established oncogenic pathways in glioblastoma. Cell *147*, 370–381.

Tam, O.H., Aravin, A.A., Stein, P., Girard, A., Murchison, E.P., Cheloufi, S., Hodges, E., Anger, M., Sachidanandam, R., Schultz, R.M., and Hannon, G.J. (2008). Pseudogene-derived small interfering RNAs regulate gene expression in mouse oocytes. Nature *453*, 534–538.

Tay, Y., Kats, L., Salmena, L., Weiss, D., Tan, S.M., Ala, U., Karreth, F., Poliseno, L., Provero, P., Di Cunto, F., et al. (2011). Coding-independent regulation of the tumor suppressor PTEN by competing endogenous mRNAs. Cell *147*, 344–357.

Wang, Y., Xu, Z., Jiang, J., Xu, C., Kang, J., Xiao, L., Wu, M., Xiong, J., Guo, X., and Liu, H. (2013). Endogenous miRNA sponge lincRNA-RoR regulates Oct4, Nanog, and Sox2 in human embryonic stem cell self-renewal. Dev. Cell *25*, 69–80.

Watanabe, T., Totoki, Y., Toyoda, A., Kaneda, M., Kuramochi-Miyagawa, S., Obata, Y., Chiba, H., Kohara, Y., Kono, T., Nakano, T., et al. (2008). Endogenous siRNAs from naturally formed dsRNAs regulate transcripts in mouse oocytes. Nature *453*, 539–543.

Yamamoto, K., Nagata, K., Kida, A., and Hamaguchi, H. (2002). Acquired gain of an X chromosome as the sole abnormality in the blast crisis of chronic neutrophilic leukemia. Cancer Genet. Cytogenet. *134*, 84–87.

Zou, M., Baitei, E.Y., Alzahrani, A.S., Al-Mohanna, F., Farid, N.R., Meyer, B., and Shi, Y. (2009). Oncogenic activation of MAP kinase by BRAF pseudogene in thyroid tumors. Neoplasia *11*, 57–65.